



## Numerical Studies of the Effect of Slope Failure on a Buried Pipeline by a Hybrid Analysis Using SPH and FEM

T. Kitano<sup>(1)</sup>, S. Fujita<sup>(2)</sup>, H. Ogura<sup>(3)</sup>, A. Suganuma<sup>(4)</sup>

<sup>(1)</sup> Professor and Dr. Eng., Nagoya University, [kitano.tetsuji@i.mbox.nagoya-u.ac.jp](mailto:kitano.tetsuji@i.mbox.nagoya-u.ac.jp)

<sup>(2)</sup> Technical Manager, Nippon Steel & Sumikin Pipeline & Engineering Co. Ltd., [fujita.shusuke.d82@nspe.nssmc.com](mailto:fujita.shusuke.d82@nspe.nssmc.com)

<sup>(3)</sup> Manager, Nippon Steel & Sumikin Pipeline & Engineering Co. Ltd., [ogura.hitoshi.xr2@nspe.nssmc.com](mailto:ogura.hitoshi.xr2@nspe.nssmc.com)

<sup>(4)</sup> Contract Researcher, Nagoya University, [suganuma@tohogas.co.jp](mailto:suganuma@tohogas.co.jp)

### Abstract

In past earthquakes, pipelines buried under roads with banking structures that are constructed across the slope of a mountain are exposed when the embankments fail. However the influence of embankment slope failure on a buried pipeline has not yet been studied. Therefore in this study, analysis of embankment slope failure is performed using smoothed particle hydrodynamics method and finite element method. The results obtained are shown below. The deformation characteristics, stress, and strain induced in the pipe that is affected by slope failure were clarified quantitatively. Furthermore, it is clarified that the exposure mechanism of the buried pipe under the slope in collapse progressing. Therefore, the results obtained by this study may contribute to earthquake countermeasures for buried pipes, and also contribute to post-earthquake recovery and aseismic design.

*Keywords: slope failure; pipeline; SPH (smoothed particle hydrodynamics method); FEM; hybrid analysis*

### 1. Introduction

Six years have elapsed since the Great East Japan Earthquake occurred in 2011. In the meantime, other earthquakes have occurred in many parts of the world. In addition, natural disasters other than earthquakes, such as floods and large-scale landslides, have occurred many times. The “Nepal earthquake” on April 25, 2015, the “Earthquake in Southern Taiwan” on February 6, 2016, and the “2016 Central Italy earthquakes” on August 24, 2016, are still fresh in our memory.

In the Hyogo-ken Nanbu Earthquake in 1995 and the Great East Japan Earthquake in 2011, middle-pressure gas welded steel pipe was exposed by a slope failure. Fig. 1 shows a damage case in the Great East Japan Earthquake. Incidentally, despite the damage, gas leakage did not occur. Regarding the welded steel pipe exposed by slope failures, the distribution of stress and strain in the pipe, and the impact on the pipe by the soil that is slipping down through the sides of the pipe, have not been discussed until now. In this paper, by using the Smoothed Particle Hydrodynamics method (SPH) and the Finite Element Method (FEM), the effects of slope failure on the buried pipe are discussed.



Fig. 1 – Exposed welded steel pipe owing to slope failure [1]

Regarding the effects of slope failure of embankment roads on a pipe that is buried under the slope, Kitano et al. [2] discussed the applicability of the following three analysis methods: the explicit dynamic finite element method, two kinds of hybrid analysis of the SPH method and the FEM. The latter two have different criteria for the conversion from finite elements to SPH particles. In the second method, time-based criteria are used as the conversion criteria. In the third method, strain-based criteria are used as the conversion criteria. The results confirmed that the third method (called SBC hereafter) is the most appropriate method for analyzing the effect of slope failure on the buried pipe, and the results of the analysis coincide with the results obtained in the field. Therefore, in this paper, by using SBC, case studies are performed for changing the strain-based criteria and the width of the excavation to initiate slope failure. The deformation behavior of the buried pipe, the stress induced in the buried pipe, and the behavior of slope failure were clarified by discussing the results of the analysis.

## 2. Method of analysis

In the numerical analysis field of geotechnical engineering, FEM incorporates a sophisticated configuration that makes it possible to estimate the deformation behavior of various ground materials. Using FEM, reproduction analyses of excavation experiments of actual large slopes have been conducted (Itoh et al. [3], Koitabashi et al. [4], Kusakabe et al. [5]). In these papers, it was confirmed that the amount of vertical displacement of the slope crest can be accurately represented up to the stage before slope failure by comparing the analytical results and experimental results. However, for methods having grids, such as FEM, it is difficult to reproduce a large deformation and collapse. For this reason, it is difficult to apply FEM to large deformation problems such as slope failure by excavation. Therefore, in the current situation, it is difficult to express a series of deformation processes of slope failure from the start to the end.

In recent years, in order to solve large deformation problems, the application of various analysis methods has been proposed. For example, in the discrete element method (DEM) (Cudall et al [6]), the ground material is modeled by a discrete body. As DEM assumes that the ground material is a discrete body, it can be easily expressed as a large deformation of the ground. However, this analysis method is based on discrete elements. Thus, it is impossible to introduce a constitutive equation that is based on continuum mechanics, which were developed and advanced in geotechnical engineering. Furthermore, as the forces between the discrete elements are regarded as a simple model, it is difficult to match the parameters obtained in the field or laboratory test and the parameters for analysis. Therefore, in order to reproduce the behavior of the ground by using this method, trial and error is required to conduct an analysis.

In addition to these calculation methods, there is a Lagrange-type analysis method that can represent a large deformation. This method is based on a continuum approximation such as the SPH method (Gingold et al. [7], Lucy [8]). This approach is a mesh-free method that does not require a computational grid, nor do the calculated points have structures. Then it is possible to express the deformation of the analysis target in a large deformation region. The advantages of the SPH method are as follows: it operates in the framework of continuum mechanics, it is based on a constitutive equation of the ground material, and it can represent a large deformation of the

ground. In addition, it is difficult to find previous studies on behavioral evaluations of buried pipeline where the SPH method was used. For more information about the SPH method in Abaqus 6.14, please refer the Abaqus 6.14 documentation (Dassault Systèmes [9]).

### 3. Analysis of embankment slope failure

#### 3.1 Model and condition of the analysis

The analysis model is shown in Fig. 2. This model was created by referring to the results of a large-scale slope excavation experiment (Itoh et al. [3]) and the results of a numerical analysis performed to confirm the reproducibility of this large-scale experiment (Nonoyama et al. [10]).

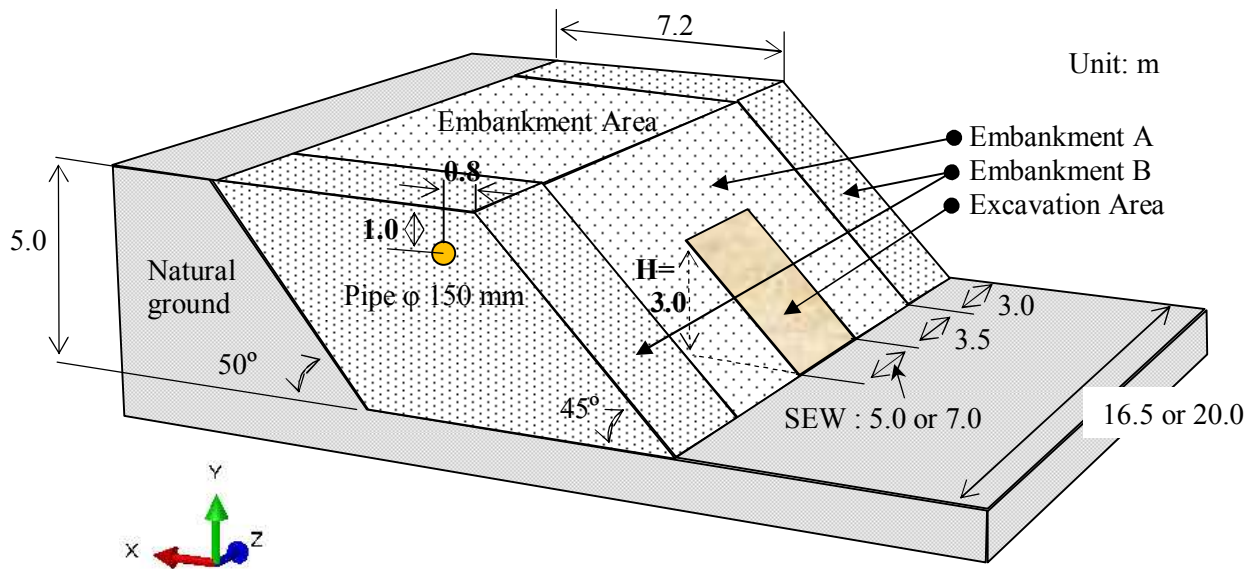


Fig. 2 – Model of the analysis

As shown in Fig. 2, the ground model is built using an embankment and foundation. The height of the crest is 5 m, and the gradient of the slope is 45°. The buried pipe was installed 0.8 m away from the top of the slope, and the depth of the pipe center from the ground surface is 1.0 m. The excavation area, with a cutting height of 3.0 m, is set at the toe of the slope to initiate a large slope failure in order to match the results of a real-scale slope excavation experiment in the field. The width of excavation for the initiation of slope failure was set to 3.5 m or 7.0 m. (Hereafter this width of excavation is denoted as SEW.) The embankment and foundation were regarded as an elastoplastic body. The soil parameters used in the analysis are shown in Table 1 (Koitabashi et al. [4], Kusakabe et al. [5]). The unit weights are the results obtained from a density test in the field. Young's modulus was determined by converting the N value obtained by a dynamic cone penetration test and Swedish weight sounding tests performed in situ. The relation between the value of N and Young's modulus indicated by Shultze (Shultze et al. [11]) was used for conversion. The adhesion and internal friction angle were determined by a box shear test.



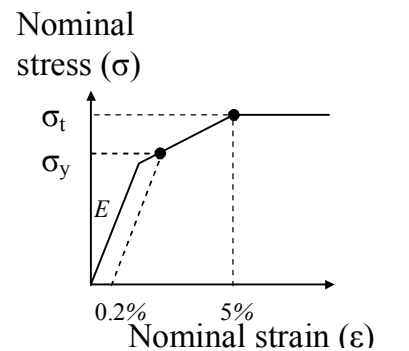
Table 1 – Soil parameters

Variables		Embankment A	Natural ground & Embankment B
Density	$\rho$ (t/mm <sup>3</sup> )	1.57E <sup>-9</sup>	2.04 E <sup>-9</sup>
Young's modulus	E (kPa)	4,512.0	8,000.0
Poisson's modulus	$\nu$	0.35	
Internal friction angle	$\phi$ (°)	35.88	5.0
Cohesion	c (kPa)	3.54	70.0
Dilatancy angle	$\psi$ (°)	0.0	0.0
Yield criteria		Mohr-Coulomb's failure criterion	

The specifications of the pipe are shown in Table 2. In this table, the nominal stress-strain relationship of the material of the pipe for this elastic-plastic model is shown. The model was designed in a trilinear fashion with minimum yield stress and a minimum tensile strength as defined in Japanese Industrial Standards (JIS). The friction coefficient between the pipe's outer surface and the surrounding ground is set as 0.3, as determined in a study by Fujita et al. [12].

Table 2 – Pipe material characteristics and dimensions

Variables		Value
Material		STPG370
Diameter	(mm)	165.2
Thickness	(mm)	7.1 (Sch. 40)
Density	$\rho$ (t/mm <sup>3</sup> )	7.8E <sup>-9</sup>
Young's modulus	E (MPa)	206,000
Poisson's modulus	$\nu$	0.3
minimum yield stress	$\sigma_y$ (MPa)	215
minimum tensile strength	$\sigma_t$ (MPa)	370
Friction coefficient between ground and surface of pipe	$\mu$	0.3 (Regarding to the contact between ground and pipe, penalty friction formulation is used.)



A schedule number indicates the approximate value of Sch. = 1000 P/S

where P = service pressure (MPa), and S = allowable stress (N/mm<sup>2</sup>)



Element division and boundary conditions of the ground and the pipe are shown in Fig. 3, and the elements are listed in Table 3.

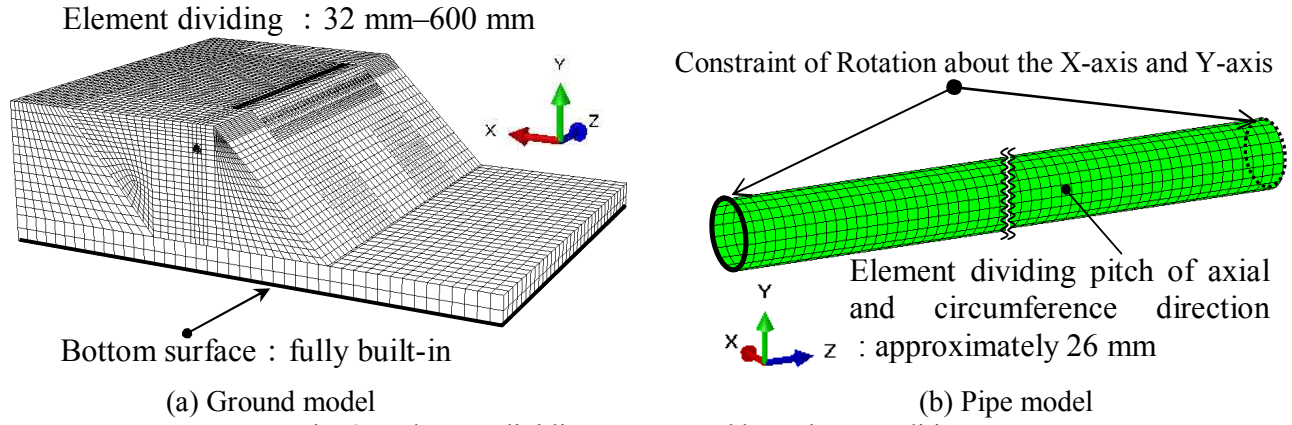


Fig. 3 – Element dividing pattern and boundary conditions

Table 3 – Elements used

	Element
Ground	(1) Natural ground and Embankment B
	Eight-node solid element, reduced integration with hourglass control (C3D8R)
	(2) Embankment A: C3D8R and continuum particle elements (SPH, PC3D)
Pipe	Four-node general-purpose shell, finite membrane strains (S4)
	Number of integration points to be used through the shell section: 5 points

### 3.2 Steps of analysis

The analysis steps are shown in Fig. 4. In step (1), a gravity loading analysis owing to self-weight is performed. Then in step (2), the excavation area is removed to initiate a slope failure. A time period of 1 s is used for gravity loading analysis at first. For the subsequent slope failure analysis, a nonlinear explicit dynamic analysis with a 4 s time period is performed.

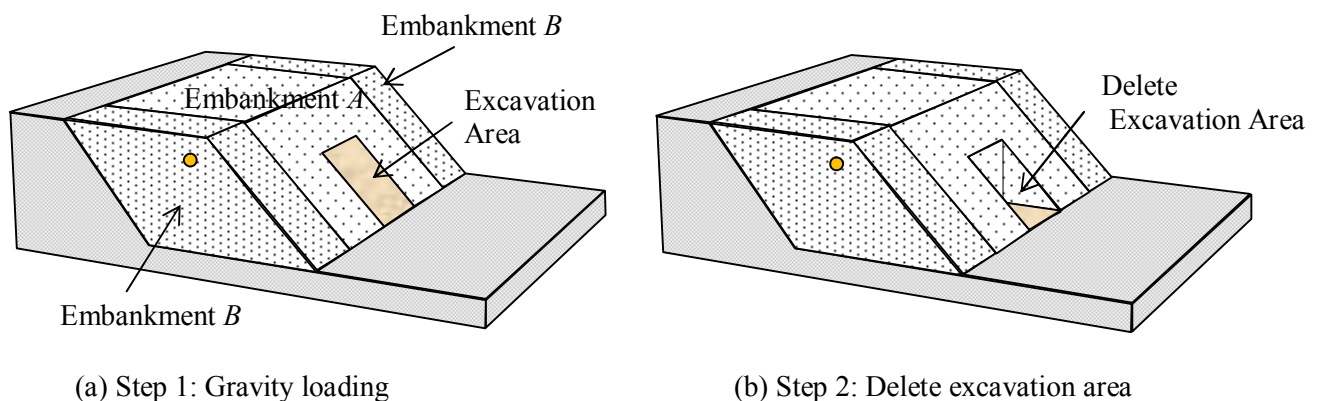


Fig. 4 – Steps of the analysis



### 3.3 Gravity loading analysis owing to self-weight

A gravity loading analysis owing to self-weight is performed to construct the initial model for slope failure analysis. At first, it was discussed how a change in magnitude of the gravitational load acting on the analysis model with time could influence the analysis model. Four types of gravitational loads with an increasing curve are tested. Those are shown in Table 4 and Fig. 5. The gravitational load is increased up to the gravity of the earth in 1 s, and then the model is left for 0.2 s to confirm the behavior of ground.

Table 4 – Increasing curve equations for gravitational load

Item	A gravitational load increasing curve equation [a: Relative load magnitude, t: Time (s)]	
Linear	$a = t$ ( $0 \leq t \leq 1.0$ )	(1)
Cubic equation	$a = t^3$ ( $0 \leq t \leq 1.0$ )	(2)
Smooth_1.0	$a = 6t^5 - 15t^4 + 10t^3$ ( $0 \leq t \leq 1.0$ )	(3)
Smooth_0.95	$a = 6\left(\frac{t}{0.95}\right)^5 - 15\left(\frac{t}{0.95}\right)^4 + 10\left(\frac{t}{0.95}\right)^3$ ( $0 \leq t \leq 0.95$ )	(4)
	$a = 1$ ( $0.95 < t \leq 1.0$ )	

Fig. 6 shows the relation between the subsidence values at the point where the maximum subsidence is obtained by the static gravity loading analysis owing to self-weight and time. A maximum subsidence of 37.59 mm is calculated by the static analysis. As shown in Fig. 6, it is recognized that the time history curve for each case is affected by the inertia force of the soil. Table 5 shows the distribution of the amount of subsidence owing to self-weight. A maximum subsidence of 37.59 mm is calculated by the static analysis. As shown in Fig. 6, it is recognized that the time history curve for each case is affected by the inertial force of the soil. Table 5 shows the distribution of the amount of subsidence owing to self-weight at the time when the gravity loading analysis owing to self-weight was finished for each gravitational-load-increasing relation. By comparing these figures, a gravitational-load-increasing curve having a linear shape is adopted in this analysis.

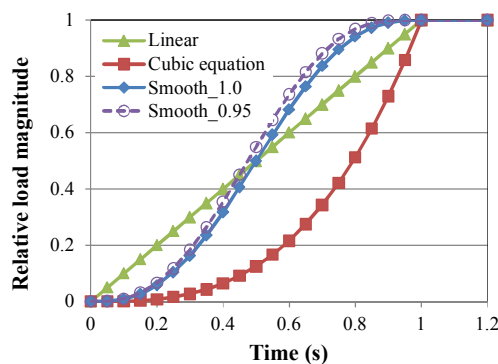


Fig. 5 – Gravitational load with time

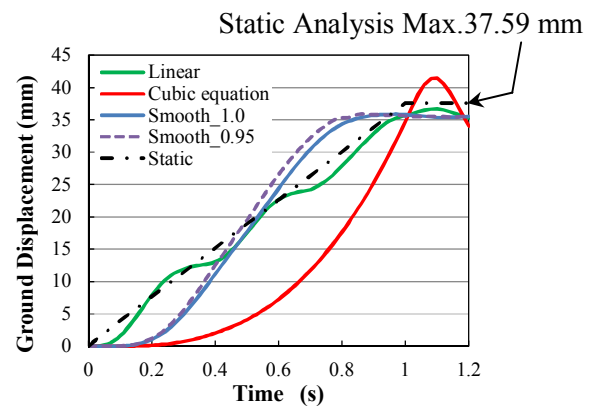
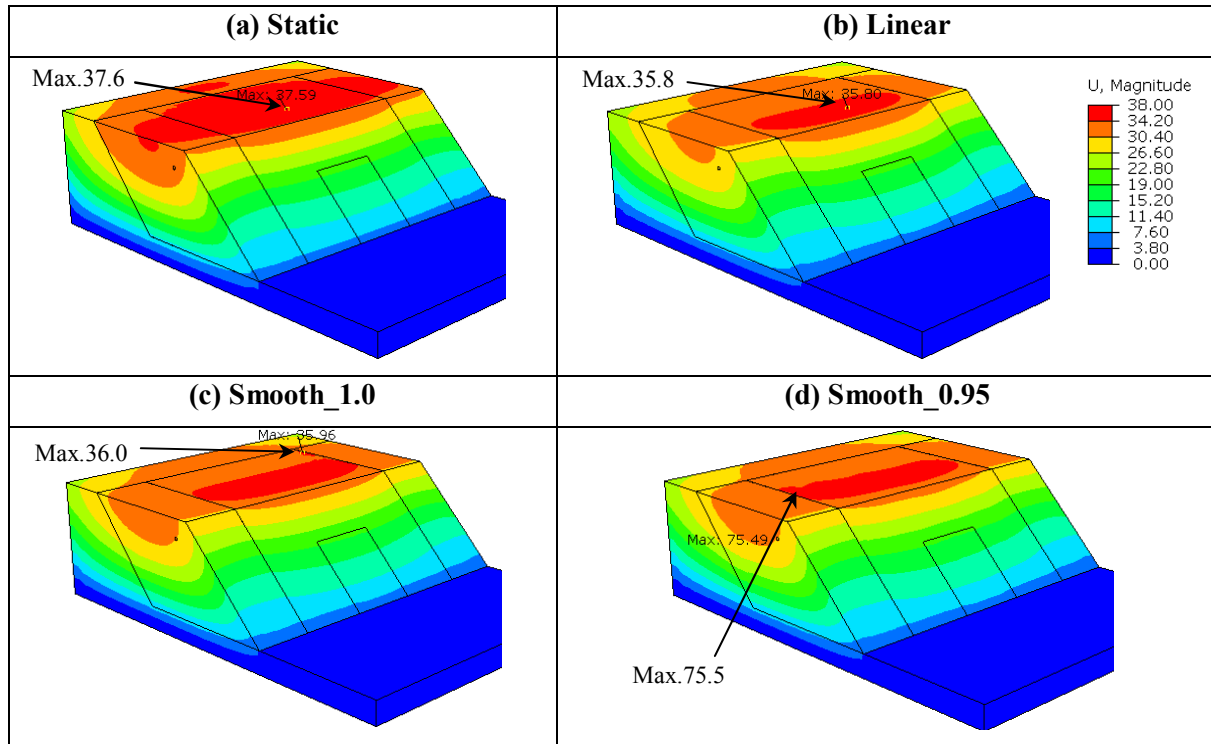


Fig. 6 – Progress of subsidence with time

Table 5 – Distribution of amount of subsidence owing to self-weight when the gravity loading analysis was finished (Unit: mm)



#### 4. Slope failure analysis

Slope failure analysis was performed up to the time when 4 s had passed from the start of slope failure. The SEW was set as 3.5 m. A pipe was buried under the slope. The results obtained are shown below.

##### 4.1 Discussion of cases

The model that was used for this analysis was created by referring to a large-scale slope excavation experiment performed in the past (Itoh et al. [3]). In an analysis using Abaqus, it is possible to convert from continuum elements to SPH particles. Analyses were conducted for the two cases shown in Table 6. By referring to a previous study by Kitano et al. [2], the continuum element for which the absolute value of the maximum principal strain exceeds the conversion criteria is converted to an SPH particle. This conversion is applied to the analysis of Embankment A, in which the collapsing part of the slope is included. For the analysis of Embankment B, the conversion to SPH particles does not apply; thus, the analysis using the continuum element is continued.

Table 6 – Criteria for converting continuum elements to SPH particles

Case	Strain-based criterion (SBC)	SEW
1	Absolute value of the maximum principal strain = 20%	3.5 m
2	Absolute value of the maximum principal strain = 30%	3.5 m

##### 4.2 Results of analysis

###### 4.2.1 Appearance of slope failure

Fig. 7 shows the appearances of the slope obtained by the analysis at the final time step for the two cases shown in Table 6. The final time step corresponds to 4 s after the initiation of slope failure. At the toe of slope failure (namely, at the part where displacement of the ground exceeds 3 m), a remarkable effect of the conversion from continuum elements to SPH particles is observed for Case 1. On the other hand, the appearances of slope failure close to the pipe are almost the same in both cases. The exposure of buried pipe can be observed clearly in the part where slope failure occurs. These appearances coincide quite well with observations of pipe exposure by slope failure that occurred in past earthquakes.

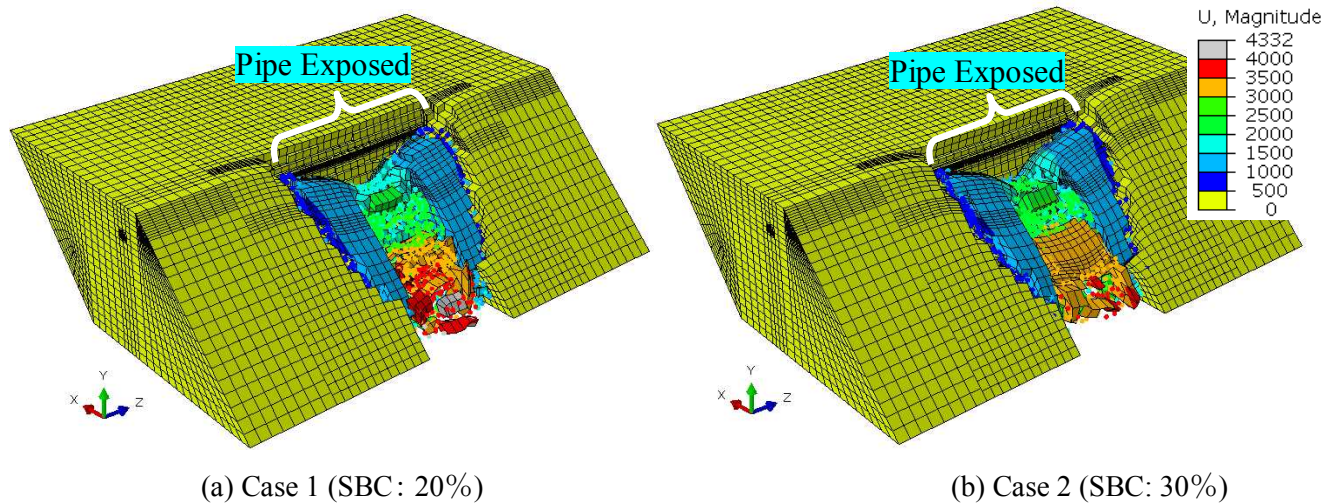


Fig. 7 – Appearance of slope at 4 s after initiation of slope failure. (Unit: mm)

#### 4.2.2 Progress of slope failure with time

The appearance of the central cross section of slope failure (namely, the X–Y plane) at 2 s after the initiation of slope failure is shown in Fig. 8 (a). The front view of the right half of the slope at the same instant is shown in Fig. 8 (b). It is recognized from Fig. 8 that the slip plane, which is circled in the figure, is created under the failing slope. The elements of the slip plane are converted to SPH particles. Regarding the progress of the slip plane, it is clarified from the results of this analysis that a breakage starts at the lower part of the excavated area and moves to the top of the slope, and a vertical crack breaks out in front of the pipeline. Then these two breakages expand and finally join together. This joining of the breakage leads to a slope failure, and the soil slips down as a clod.

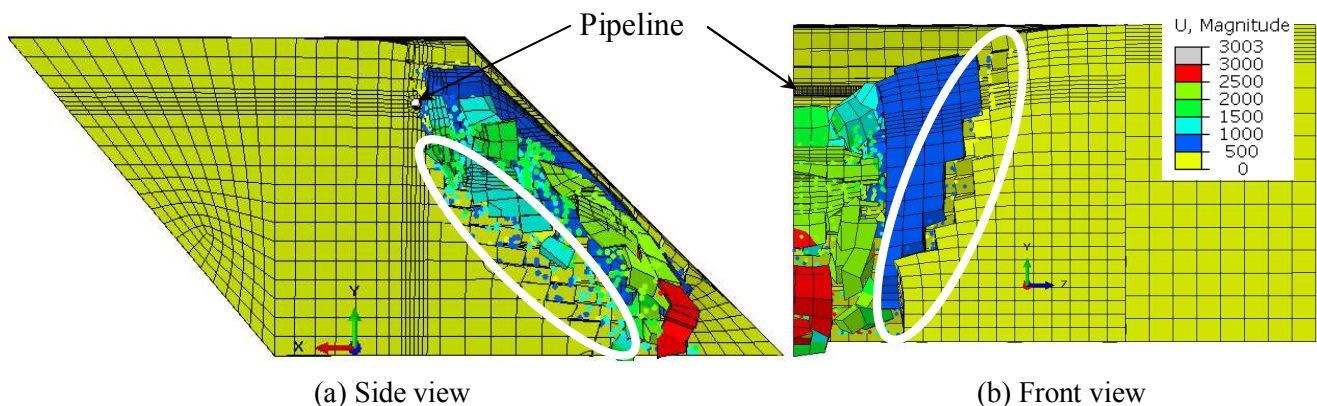


Fig. 8 – Appearance of slope failure at 2 s after initiation of slope failure for SBC: 20%. (Unit: mm)



Fig. 9 shows the appearance of the progress of the failure with time. Fig. 9 (a), (b), and (c) show the appearance at 1 s, 2 s, and 4 s after the initiation of the failure. The displacement of the ground is more than 4 m at 4 s after the initiation of the failure. For the ground around the pipeline, remarkable changes cannot be observed beyond 2 s after the initiation of slope failure. In this stage, the buried pipeline suppresses the soil behind it. Then the soil behind the pipeline tends to become stable.

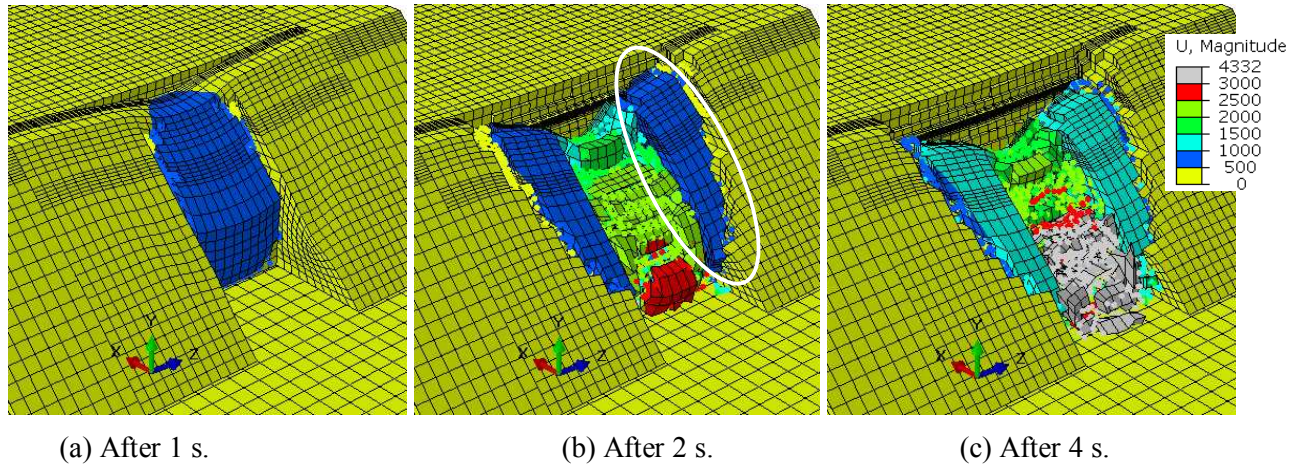
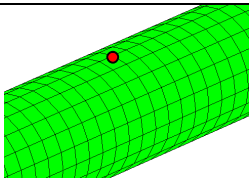
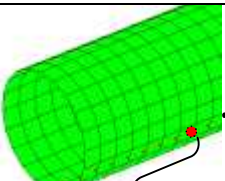


Fig. 9 – Change of appearance at indicated time after initiation of failure (SBC: 20%, Unit: mm)

#### 4.2.3 Deformation of the buried pipe and stress induced

Table 7 shows the relationship between the nodal point and the figures that show the deformation of the pipe or the stress distribution in the pipe. Fig. 10 shows the relation between the Mises stress induced at the top of the buried pipe in the central section of slope failure as shown in Table 7, and the time from the initiation of the failure. The value of the Mises stress increases waveringly, and attains an almost constant value at 2 s after the initiation of slope failure in the cases of SBC: 20% and SBC: 30%. This change in stress with time agrees with the progress of slope failure and also the change in the deformation of the pipe, with the time as shown below. Fig. 11 shows the distribution of longitudinal stresses induced at the lowest part of the pipe, as shown in Table 7, at the respective times. The curve that is indicated at a time of 0 s corresponds to the stress distribution at the end of the gravity loading analysis owing to self-weight. The change of stress in the vicinity of the boundary between Embankment A and B at the time of 0 s is caused by the differences in the soil characteristics of each embankment. The displacement of the pipe in the central section of the slope shows its maximum value.

Table 7 – Relation between nodal point and figures showing the results

	Top of pipe in central section	Group of points at lowest part of pipe
Fig.	Fig. 10	Fig. 11–13, 15–17
points		 approx 25-cm pitch

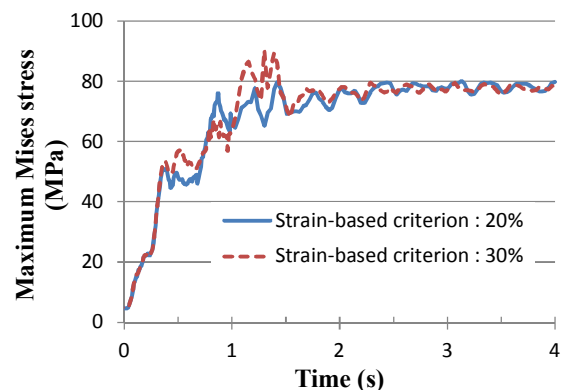
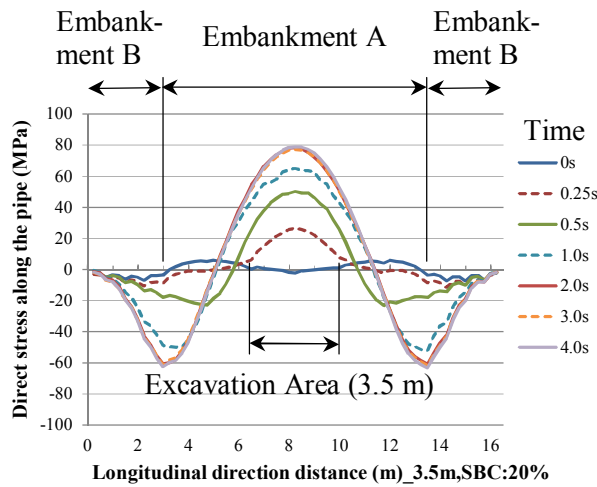
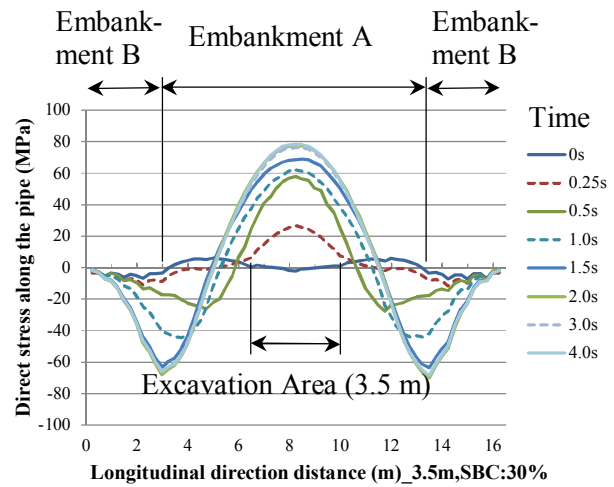


Fig. 10 – Change in Mises stress at top of pipe in central section with time.



(a) SBC: 20%



(b) SBC: 30%

Fig. 11 – Distribution of stress along pipeline at respective times

The stresses induced in the pipe on both the compressional side and tensile side increase as slope failure progresses. However, after 2 s from the initiation of failure, the increase in stress is not so large, and the stress values tend to become stable. From the results shown in Fig. 10 and Fig. 11, the differences in the value of SBC show almost no effect on the stress induced in the pipeline. Fig. 12 and Fig. 13 show the displacement of the pipeline. The maximum displacement is observed at the center of slope failure. The progress of the displacement is smooth.

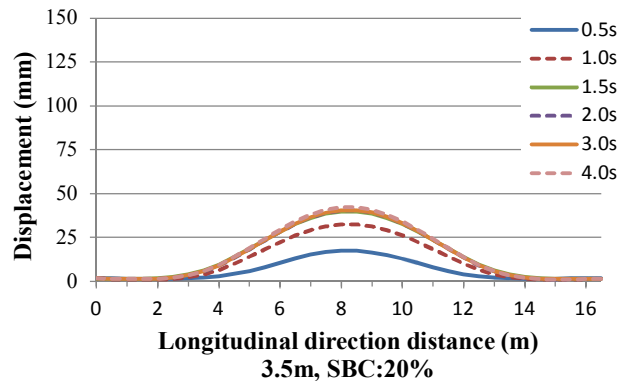


Fig. 12 – Distribution of displacement along pipeline at respective times

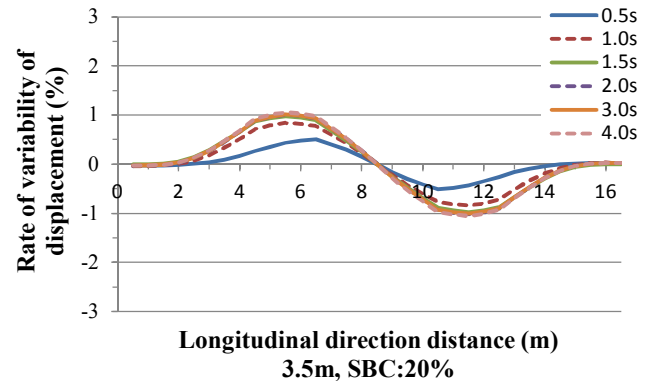


Fig. 13 – Distribution of rate of variability of displacement along pipeline at respective times

#### 4.3 Study of the mesh size of the ground model

In order to discuss the effect of the mesh size of the ground model, the analysis was carried out for the ground model having some fine size meshes. To facilitate failure of the surrounding ground of the pipe, the ground immediately above and behind (the side opposite to the inclined surface) of the pipe are modeled by fine meshes. As the results, the calculation was diverged when it passed for 2.05 seconds since slope failure started. However, the following two points have been confirmed from the analysis results up to the 2.05 seconds. Therefore, it is considered that the standard size mesh is reasonable at the moment.

- (1) In the case of the model having fine meshes, by the progress of the failure of the ground in the vicinity of the pipe, earth pressure acting on the pipe is increased.
- (2) On the other hand, a calculation is unstable. The reason is that the conversion from FEM element to SPH particle suddenly occurs and failure happens intensely.

## 5. Analysis for enlarged width slope failure

### 5.1 Discussion of cases

A slope failure analysis is performed for the case in which the SEW is enlarged from 3.5 m to 7.0 m. The conditions for the analysis are shown in Table 8. The other conditions are the same as those of the previous analysis.

Table 8 – Finite element conversion to SPH particles for SEW of 7.0 m

Case	Strain-based criterion(SBC)	SEW
3	Absolute value of the maximum principal strain = 20%	7.0 m

### 5.2 Results of analysis

Fig. 14 shows the appearance of the slope at 2 s after initiation. By comparing the appearance of the SEW having a width of 3.5 m shown in Fig. 9 (b), it is recognized that the progress of the failure is faster and the area of failure is larger. On the other hand, it is recognized that there is almost no difference in the displacement of the ground on both sides of the failure. The area is circled in Fig. 14. Fig. 15 show the longitudinal stress distribution induced in the buried pipeline. A maximum stress of 150 MPa can be recognized. It is confirmed that this maximum stress is less than the yield stress of the pipe, which is 215 MPa. It is recognized from the stress distribution that the distributed load is imposed from behind the pipeline. Fig. 16 shows the displacement of the pipeline. The amount of displacement of the pipe increases owing to the elongation of the width of slope failure. A maximum displacement of approximately 150 mm is obtained.

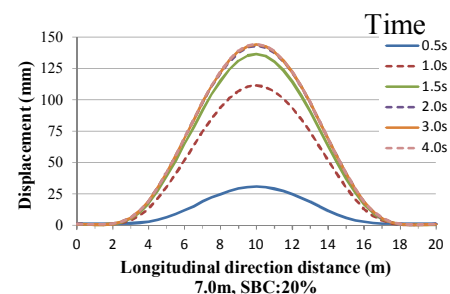
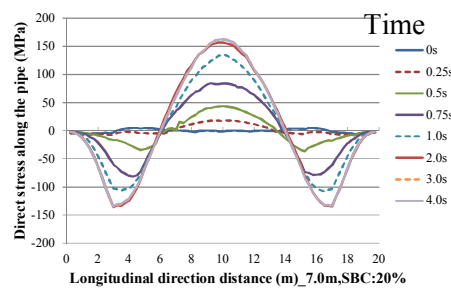
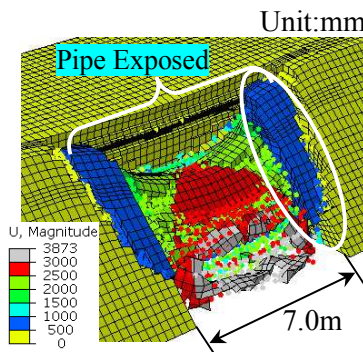


Fig. 14 – Appearance at 2 s after

Fig. 15 – Stress along the pipeline

Fig. 16 – Distribution of displacement

## 6. Conclusion

- (1) It is confirmed that the longitudinal stress induced in the buried pipeline by a slope failure is less than the yield stress of the pipe. In this study, an analysis of the effects of soil movement behind the pipeline, which will slip down the sides of the pipeline, is not performed. However, judging from the standpoint of the stress induced in the pipeline, the downward slippage of the soil through the sides of the pipe tends to decrease the stress in the pipeline. Therefore, it is considered that the stress seen in this study may be larger than the stress induced in the pipeline by the soil slipping downward.



- (2) The mechanism of the exposure of buried pipeline under the slope is clarified. Furthermore, it is confirmed that a clod of soil is created by the joining of a slip plane and a crack. The slip plane starts from the toe of the slope and extends toward the top of the slope, and the crack breaks out vertically on the slope surface in front of the buried pipeline. This progress of exposure of the buried pipeline coincides quite well with the actual pipeline exposure caused by the Great East Japan Earthquake.
- (3) It is confirmed that the movement of soil in the progress of a slope failure can be analyzed using a hybrid analysis method that combines SPH and FEM. Furthermore, this makes it possible to clarify the deformation of the pipeline and the stress and strain induced in the pipeline with the progress of slope failure in which the pipeline is buried.
- (4) It is confirmed that the behavior of the buried pipeline that is suffering slope failures is similar to that suffered by the liquefaction and side movement of the ground.

## 7. Acknowledgements

We would like to express our sincere appreciation to Assistant Professor Hideto Nonoyama at National Defense Academy for his very useful advice and suggestions. This work was supported by JSPS KAKENHI Grant Number 15K12489.

## 8. References

- [1] Ministry of Economy, Trade and Industry (2012): *Report on disaster prevention methods based on lessons learned from the Great East Japan Earthquake*, The Japan Gas Association, Japan. (in Japanese)
- [2] Kitano, T., Fujita, S., Ogura, H., and Suganuma, A. (2016): "Failure analysis of embankment slope under which a pipeline is buried and influence evaluation of the pipeline by slope failure," *UESI Pipelines Conference 2016*, Kansas City, Missouri, USA.
- [3] Itoh, K., and Toyosawa, Y. (2009): "Field test of slope failure during slope cutting work," *Journal of Japan Society of Civil Engineers, Ser. C (Geosphere Engineering)* 65(1), 254–265. (in Japanese)
- [4] Koitabashi, T., Suemasa, N., Itoh, K., and Toyosawa, Y. (2008): "Mechanism of slope failure caused by toe excavating," *Proceedings of the Japan National Conference on Geotechnical Engineering: The 43th Japan National Conference on Geotechnical Engineering* 435, 869–870. (in Japanese)
- [5] Kusakabe, S., Koitabashi, T., Suemasa, N., Itoh, K., Tamrakar, S.B., and Toyosawa, Y. (2006): "Field test related to slope failure during slope cutting work (Part 3. Numerical analysis)," *Proceedings of the Japan National Conference on Geotechnical Engineering, The 41th Japan National Conference on Geotechnical Engineering* 480, 959–960. (in Japanese)
- [6] Cudall, P.A., and Strack, O.D.L. (1979): "A discrete numerical model for granular assemblies," *Geotechnique* 29(1), 47–65.
- [7] Gingold, R. A., and Monaghan, J.J. (1977): "Smoothed particle hydrodynamics: theory and application to non-spherical stars," *Royal Astronomical Society Monthly Notices* 181, 375–389.
- [8] Lucy, L.B. (1977): "A numerical approach to the testing of the fission hypothesis," *The Astronomical Journal* 82(12), 1013–1024.
- [9] Dassault Systèmes (2014). Abaqus 6.14 Documentation.
- [10] Nonoyama, H., Sawada, K., Moriguchi, S., Yashima, A., and Itoh, K. (2012): "A 2D SPH simulation for real-scale slope excavation experiment," *Japanese Geotechnical Journal* 7(4), 543–555.
- [11] Schultze, E., and Menzenbach, E. (1961): "Standard penetration test and compressibility of soil," *Proc. 5th ICSM* 1, 527–532.
- [12] Fujita, S., Ogura, H., Kitano, T., and Nonaka, T. (2014): "A study of deformation analysis using solid and shell elements for buried steel pipeline," *Proceedings of the 14th Japan Earthquake Engineering Symposium, Japan Association for Earthquake Engineering*, 3767–3772. (in Japanese)